Indian Journal of Advances in Chemical Science

Article

Synthesis, Crystal Structure, and Characterization of Manganese-Metal-Organic Framework with Improved Electrocatalytic Activity for Supercapacitor Application

G. Krishnamurthy*, B. M. Omkaramurthy

Department of Studies in Chemistry, Bangalore University, Central College Campus, Bengaluru - 560 001, Karnataka, India

ABSTRACT

A manganese metal-organic framework (Mn-MOF) has been synthesized using a low-temperature solvothermal procedure in the presence of terephthalic acid and 1-methylimidazole in dimethylformamide. The crystal structure studies were made and found that the molecule has a three dimensional framework in which the θ ranges from 5.942 to 50 with monoclinic I2/a space group. The final full matrix least-square refinement over F^2 is converged on $R_1 = 0.0558$, $wR_2 = 0.1696$ through goodness-of-fit = 1.095. The surface area of the Mn-MOF has been measured by Brunauer–Emmett–Teller method and the surface area was found to be 1.2352 m^2/g. The average pore diameter and pore volume were about 2.6 nm and 0.00569 cc/g, respectively. The electrochemical studies were made by cyclic voltammetry, galvanostatic charge-discharge, and electrochemical impedance spectroscopy techniques and found that the Mn-MOF has high charge storage capacity up to 4000 Fg^{-1}, which reflects the supercapacitor behaviour of the material. Also Mn-MOF material exhibits the energy density up to 500 ($Whkg^{-1}$) and the power density of about 0.125 (Wkg^{-1}). These values imply that the Mn-MOF can be an efficient material for electrochemical supercapacitor/other energy storage application.

Key words: Manganese metal-organic framework, Secondary building units, Solvothermal synthesis, Supercapacitor, Cyclic voltammetry.

1. INTRODUCTION

Metal-organic frameworks (MOFs) are more fascinating porous solids formed from diverse molecular complexes. The fabrication of new MOFs with appropriate size and porosity, etc., is a challenging aspect in the coordination chemistry as these MOFs exhibit interesting topological description and visual structures [1]. Accordingly, they are characterized by a wide number of potential applications such as chemical/bio-sensor, heterogeneous catalysis, [2] molecular magnetism, [3] photoluminescent property, [4] and gas storage [5]. In general, MOFs are built by coordinated metal clusters and organic linkers [6]. The MOFs can be synthesized either by hydrothermal, solvothermal, or microwave, techniques, and the like. These methods involve normally elevated temperatures and pressures [7]. The novel MOFs can be fabricated by the alteration of secondary building units (SBUs) and using preferring organic linkers. The use of octahedral, triangular shaped SBUs to build exciting frameworks in suitable solvent systems is quite desirous [8]. MOFs can be produced by several high-yield synthesis procedures and economically by low-temperature solvothermal method, usage of the microwave, ultrasonic, electrochemical [9], etc. Recently, solvothermal synthesis technique has gained much of the interest due to the formation of tuneable structures of MOFs [10]. Even though a large number of MOFs were synthesized by this method, equivalent MOFs were also produced using either static inorganic ions or organic molecules, the identical templates [11]. Recently, MOFs have gained growing interest as a new energy storage electrode material, but the low capacity of the best MOFs' materials has mainly prevented the expression of their functions [12]. Enormous effort has been devoted to the study of diverse approaches to improve the hydrogen uptake into the porous MOFs [13-19]. The world DOEs destination used for hydrogen storage is schemes working at significant close-atmospheric pressures and temperatures [20]. MOFs have also drawn greater interest due to their structural and functional properties as the potential candidates for sensing the chemical/biological species [21]. However, numerous factors such as statistical principle, temperature, concentration, pH, and solvent polarity must be considered while synthesizing a novel MOF. In this study, the synthesis of (Mn[Tpa][Mi][dimethylformamide (DMF)]) MOF has been carried out by solvothermal technique using two organic ligands, including terephthalic acid and methylimidazole, and Mn $(NO_3)_2$ as a manganese precursor. The solvothermal synthetic routes described in this work allow us to obtain a novel Mn-MOF with the coordination modes of the carboxylate groups that give rise to an extraordinary crystal with a unique three dimensional (3D) structure. The product was characterized using powder X-ray diffraction (PXRD), field emission scanning electron microscope (FE-SEM), Fourier-transform infrared spectroscopy (FT-IR), nitrogen adsorption/desorption (Brunauer–Emmett–Teller [BET]) studies, and electrochemical measurements. The obtained Mn-MOF has exhibited superior electrochemical charge storage property.

***Corresponding author:**
E-mail: drgkmurthy.bub@gmail.com

ISSN NO: 2320-0898 (p); 2320-0928 (e)
DOI: 10.22607/IJACS.2019.701002

Received: 30th November 2018;
Revised: 15th November 2018;
Accepted: 19th December 2018

2. EXPERIMENTAL

2.1. Materials and Methods

All the chemicals such as manganese nitrate hexahydrate, terephthalic acid, N, and N-DMF used in this research work were of analytical grade, and obtained from SDFCL (SD Fine Chem. Limited), and 1-methylimidazole and chloroform were obtained from Spectrochem Pvt., Ltd. All of these were reagent grade chemicals and used as they received. The reactors used were stainless steel autoclaves with Teflon liners of 60 ml capacities. The Matri (Kerala) hot air oven was used for heating the autoclaves. S V Scientific Sonicator was used for uniform dispersion of the reaction solution. All the electrochemical characterization and measurement experiments were carried out in CHI 608E electrochemical analyzer with the three-electrode system.

2.2. Synthesis of Mn-MOF

A mixture of Mn $(NO_3)_2.6H_2O$ (1.0 g) and terephthalic acid (0.70 g) were dissolved separately in 15 ml of DMF with mild stirring and then added to 0.5 ml of 1-methylimidazole to get a clear solution. The resulting solution was transferred to an autoclave and heated in an oven at 120°C for 72 h (Figure 1). The reaction system was then allowed to cool down to room temperature. The obtained shiny white colored crystalline material was filtered and repeatedly washed through fresh DMF several times, followed by chloroform. Finally, the product was dried at room temperature for 24 h.

2.3. Characterization Techniques

The resulting product was characterized by studying the vibrational properties of the functional groups of Shimadzu 8400S FTIR spectrophotometer using KBr pellets within the range of 400–4000 cm^{-1}. PXRD study has been carried out using Bruker D8 Advance X-ray powder diffractometer with CuKα radiation, at λ = 0.1541874 nm to obtain information on the nature of the product (crystalline or amorphous), phase structure and purity of the product. FE-SEM images were taken on the Zeiss FE-SEM. The specific surface area, pore volume, and pore structure of the materials were calculated using the BET technique on Nova 1000 instrument. The crystal information data were collected at 293 K Using Olex2 instruments. The structure was solved with the ShelXT structure solution program using ShelXL refinement package with (conjugate gradient least squares [CGLS]) minimization. All the electrochemical characterization and measurement experiments were performed with CHI 608E electrochemical analyzer with the three-electrode system consisting of a bare carbon paste electrode (BCPE) or modified carbon paste electrode as working electrode, the platinum wire as auxiliary or counter electrode and Ag/AgCl as a reference electrode.

3. RESULTS AND DISCUSSION

3.1. Structural Description

A single crystal data of (Mn[Tpa][Mi][DMF]) were collected on a Nova diffractometer. The crystal was set aside at 293 K during data collection. Using Olex2, the structure was solved through ShelXT. The structure resolution programs to uses refining and intrinsic phase by the ShelXL refinement package using CGLS minimization. Mn-MOF is made up of 3D frameworks based on SBUs. The range of θ was from 5.942 to 50. The structure was solved in the monoclinic I2/a space group (Table 1). The entire non-hydrogen atoms were distinguished by an anisotropically; the Mn-MOF contains both terephthalic acids and 1-methylimidazole groups in the asymmetric unit (Figure 2a). This crystal structure includes two types of manganese ions with different coordination environments (Figure 2b). The issue must exist well-known such former following description data are steady through the crystal structure. The final full matrix least-squares refinement over F^2 converged on R^1 = 0.0558, wR^2 = 0.1696 through goodness-of-fit = 1.095.

The Cambridge Crystallographic Data Centre (CCDC) number of the material is 1,564,429, which provides the supplementary crystallographic data for this paper.

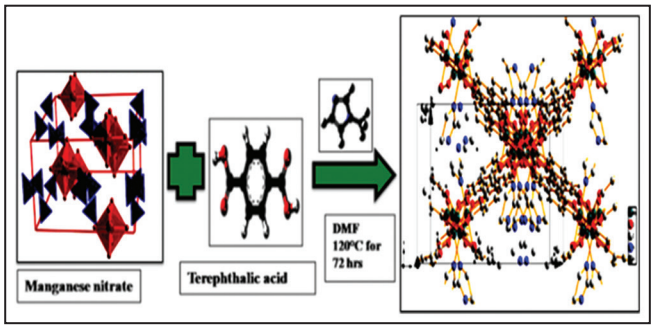

Figure 1: Schematic representation of the formation of manganese metal-organic framework.

Table 1: Structural analysis and crystal data refinement for Mn-MOF.

Empirical formula	$C_{15}H_7Mn_{1.5}N_2O_6$
Formula weight	393.64
Temperature/K	293 (2)
Crystal system	Monoclinic
Space group	I2/a
a/Å	17.9240 (6)
b/Å	9.6109 (3)
c/Å	19.1656 (6)
α/°	90
β/°	95.602 (3)
γ/°	90
Volume/$Å^3$	3285.81 (18)
Z	8
$\rho_{calc}g/cm^3$	1.591
μ/mm^{-1}	1.203
F (000)	1572.0
Crystal size/mm^3	0.20×0.11×0.10 mm^3
Radiation	Mo Kα (λ=0.71073)
2Θ range for data collection/°	5.942–50
Index ranges	$-19\leq h\leq 21$, $-11\leq k\leq 11$, $-21\leq l\leq 22$
Reflections collected	11188
Independent reflections	2900 (R_{int}=0.0434, R_{sigma}=0.0404)
Data/restraints/parameters	2900/0/222
Goodness-of-fit on F^2	1.095
Final R indexes (I≥2σ[I])	R_1=0.0558, wR_2=0.1696
Final R indexes (all data)	R_1=0.0631, wR_2=0.1777
Largest diff. peak/hole/e$Å^{-3}$	1.69/−0.81

Mn-MOF: Manganese metal-organic framework

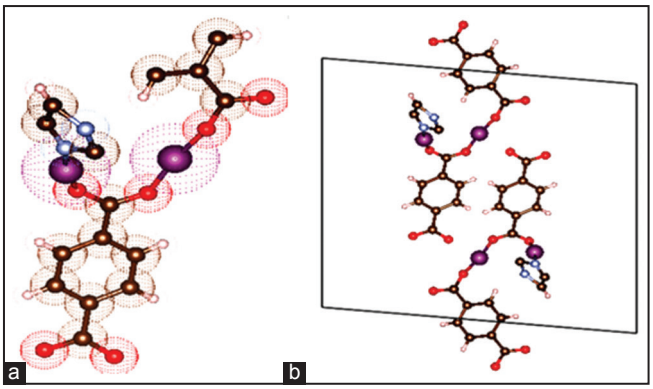

Figure 2: (a) Crystal structure of Manganese[Mn][Tpa][Mi] [dimethylformamide] and (b) coordination environment around Mn center is indicated. The atomic labeling is given for atoms in the asymmetric unit. Color code: Manganese – purple, carbon-black, Nitrogen-blue, oxygen – red, hydrogen – gold.

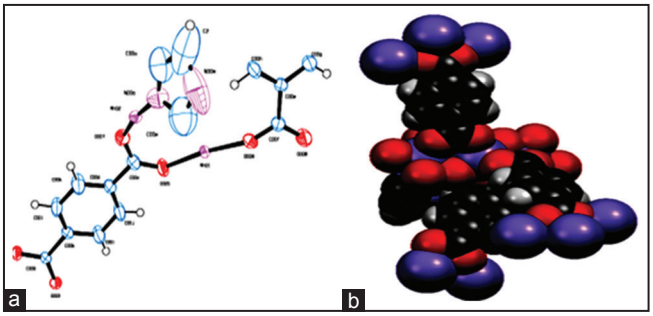

Figure 3: (a) and (b) are the Oak Ridge Thermal Ellipsoid Plot and space filled diagram of Manganese[Tpa][Mi] [dimethylformamide], respectively.

The asymmetric unit consists of two Mn^{2+} ions, one Tpa and MI ligands are coordinated with DMF molecules to show with Oak Ridge Thermal Ellipsoid Plot (Figure 3a) and space filled diagram (Figure 3b) of Mn-MOF. Manganese is coordinated with three oxygen atoms from three carboxylate groups and two coordinated DMF molecules in an octahedral geometry. The Mn-MOF was anisotropic thermal parameters with refined on I2/a space group. Every hydrogen atom was produced tentatively against the specific atoms and fixed thermal factors of refined anisotropy. It ought to be famous that solvent molecules in the structure were irregularly isolated and thus complicated to refine by discrete-atom models. This may be attributed to the bulky channels of ensuing in the puny contacts with uncoordinated DMF molecules; hence, some atoms of DMF molecules with reduced thermal parameters are reserved and refined anisotropically. In Mn(II) ion is connected by two imidazole and two carboxylate groups, and each group links three trimers to form a 3D frameworks (Figure 4a), précised along with X, Y, and Z-axis to form one-dimensional, two-dimensional, and 3D channels with a diameter of ~17 Å (Figure 4b and 4c).

3.1.1. Bond lengths and bond angles of Mn-MOF

Mn-MOF formed by four oxygen atoms from two Tpa and two Mi ligands (Figure 2). The Mn1-O bond lengths range from 1.261(5) to 2.400(3) Å (Table 2) can be regarded as normal for this type of coordination environment. The strong distortion of the trigonal prism, reflected by angles varying from 44.6 (6) to 169.08° (16)° (Table 3) is most likely due to the coordination of both a chelating carboxylate group.

3.2. FT-IR Spectral Analysis

FT-IR is an important technique to identify the presence of functional groups and or the interaction between the metal and organic ligands in Mn[Tpa][Mi][DMF] samples. The FTIR spectrum is shown in

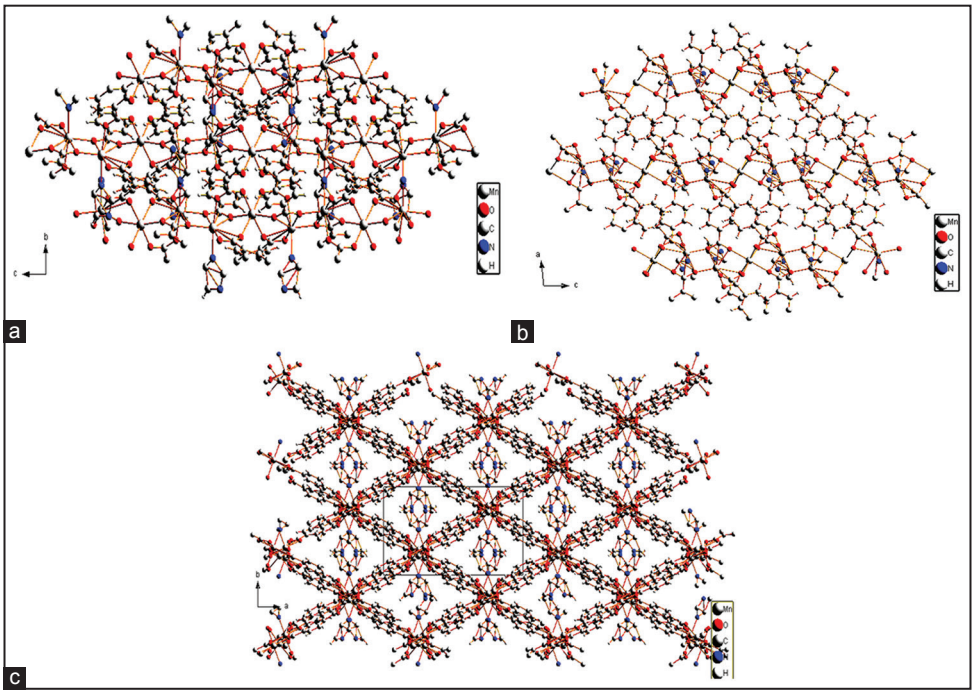

Figure 4: (a) View of the coordination environment of manganese metal-organic framework (Mn-MOF) thermal ellipsoids is drawn at the 50% probability level. Oxygen molecules and hydrogen atoms have been omitted for clarity (symmetry codes: [1]1/2+X, 1−Y, +Z; [2]1−X, 1−Y, 1−Z; [3]3/2−X, +Y, 1−Z; the one-dimensional right-handed helical chain of Mn-MOF. (b) A two-dimensional layer composed of right-handed helical chains through O-H-O hydrogen bonds. (c) The three-dimensional structure generated for Mn-MOF (white-C, blue-N, red– O, cyano- Mn, and light gray-H).

Table 2: Selected bond lengths of Mn-MOF.

Atom	Atom	Length/Å
Mn01	O003[1]	2.303 (3)
Mn01	O003[2]	2.303 (3)
Mn02	O003[2]	2.400 (3)
Mn02	O004[4]	2.188 (3)
O003	Mn01[1]	2.303 (3)
O004	Mn02[6]	2.188 (3)
O004	Mn02[5]	2.305 (3)
O005	C00C	1.261 (5)
O006	C00F	1.269 (6)
O007	C00C	1.251 (6)
O008	Mn02[3]	2.182 (4)
N00A	C00O	1.254 (11)
N00A	C00P	1.372 (12)
C00B	C00I	1.389 (6)
C00C	C00D	1.509 (6)
N00M	C00O	1.915 (14)
C00O	C00P	1.906 (18)

Mn-MOF: Manganese metal-organic framework

Table 3: Selected bond angles of Mn-MOF.

Atom	Atom	Atom	Angle/°
O003[1]	Mn01	O003[2]	169.08 (16)
O005	Mn01	O003[2]	91.10 (12)
N00A	Mn02	O003[1]	89.54 (16)
N00A	Mn02	O004[4]	96.32 (16)
Mn01[2]	O003	Mn02[5]	96.20 (10)
Mn02[6]	O004	Mn02[5]	103.50 (11)
C009	O003	Mn01[2]	158.4 (3)
C009	O003	Mn02[5]	90.3 (2)
N00A	Mn02	O004[4]	96.32 (16)
Mn01[2]	O003	Mn02[5]	96.20 (10)
C009	O003	Mn01[2]	158.4 (3)
C009	O003	Mn02[5]	90.3 (2)
Mn02[6]	O004	Mn02[5]	103.50 (11)
N00M	C00P	N00A	110.4 (11)
C2	C00O	N00M	44.6 (6)

Mn-MOF: Manganese metal-organic framework

Figure 5. The broad absorption band centered at 3250–3000 cm^{-1} is attributed to the existence of hydrogen-bonding connections between the frameworks. The presence of two strong peaks ranges of 1513 and 1369 cm^{-1} could be ascribed for the mass (OCO) and ms (OCO) stretching vibrations of the Tpa. The aromatic nucleus [m(C-C), m(C-N)] is close to 1662 cm^{-1}, while m(C-H) bend vibrations are about 829 and 744 cm^{-1} (phenyl) confirms the presence Mn-O bind. The shifting of the C=O of carboxylate and C-N vibrations indicates the formation of the bonding with the metal Mn centrally with the ligands terephthalic acid and methylimidazole.

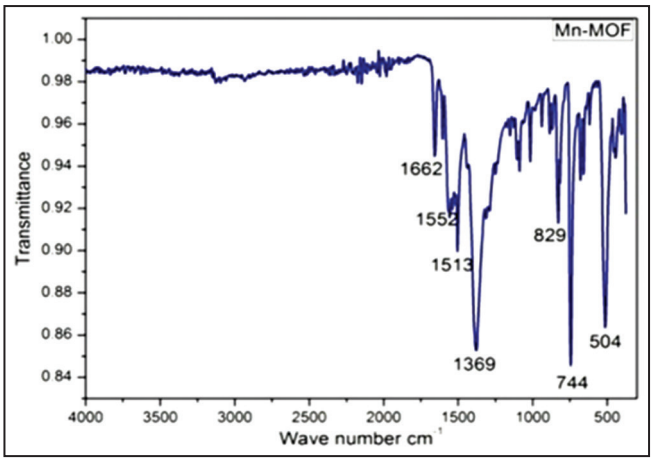

Figure 5: Fourier-transform infrared spectroscopy spectrum of as prepared manganese metal-organic framework compound.`

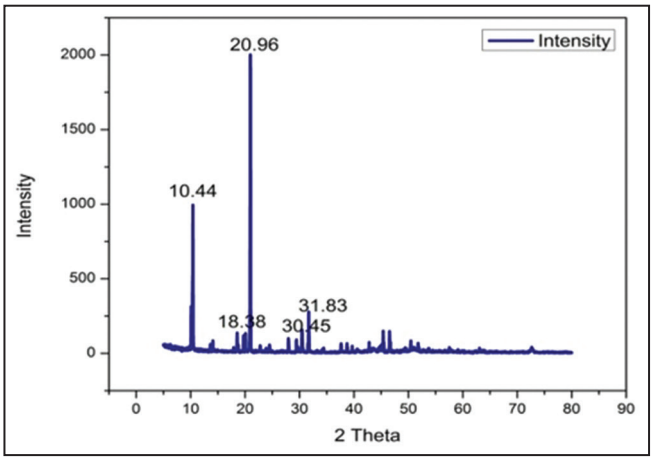

Figure 6: Powder X-ray diffraction patterns for manganese metal-organic framework compound.

3.3. PXRD Analysis

X-ray powder diffraction (PXRD) is a technique, which reveals the information about the nature of crystal structure and phase purity of the sample. The X-ray powder diffraction pattern (Figure 6) shows the sharp peaks of the pattern, which indicates the crystalline nature of the material. The presence of the prominent metallic peak at the 2θ values at 10.43 and 20.97 indicates the coordination of metal with the ligands to form a complex. This pattern of much of noise and extra peaks hint us about the phase structure and purity of the products obtained. The theoretical (simulated) PXRD pattern calculated from the single-crystal XRD data is in good conformity with the experimental pattern. This confirms that the resulting phase is pure and highly crystalline. These results are consistent through the larger crystallite size and also an excellent crystalline nature can be seen.

3.4. FE-SEM Analysis

The surface was characterized using FE-SEM images of Mn-MOF. The FE-SEM imaging to enable the study of the microstructure and surface morphology of the products. The micrographs (Figure 7) show the particles distribution in a range of dimensions like diamond shaped crystals. The FE-SEM images viewed under high and low (at 100 μm and 20 μm) magnifications. The images show the free particles of diamond-like crystals with attractive smooth surfaces.

3.5. Energy Dispersive X-ray (EDX) Analysis

Figure 8 shows the EDX pattern of Mn-MOF. The EDX pattern confirms the presence of manganese, carbon, and oxygen along with their composition. The composition of the element (weights%) is carbon (48.84), oxygen (26.20), and manganese (24.97).

3.6. BET Surface Area Measurement

The surface area, pore size, and pore volume of Mn-MOF were evaluated through N_2 adsorption using a NOVA-1000 BET surface area measurement instrument. Materials were degassed at 180°C for 4 h. Surface areas of Mn-MOF were evaluated using non-local density functional theory. The BET specific surface area, pore textural properties, the cumulative pore volume, average pore diameter, and the Langmuir specific surface area for the Mn-MOF were calculated. The sorption isotherms obtained with nitrogen gas signify type I isotherm with no hysteresis, which demonstrates the presence of the microporous structure (Figure 9). Obtained BET surface area is about 8.760 m^2/g, which represents the adsorption capacity of our compounds. The adsorption capacity reaches (the amount adsorbed) the value of about 1.273 m^2/g and the average pore diameter of about 25.967Å, which corresponds to micropore volume, 0.00569 cc/g.

3.7. Thermogravimetric Analysis (TGA)

Thermogravimetric measurement on the compound was made under the N_2 atmosphere at a heating rate of 20°C/min without pre-treatment (Figure 10). Figure 10 shows the weight loss at two points. First weight loss was observed between the temperature 250 and 300°C and the second weight loss was observed in the range 350–450°C. The first weight loss of about 18% in the range 250–300°C could be attributed to the loss of free DMF molecule. The second weight loss of about 36% was observed in the range of temperature 350–450°C, which could be due to the cleavage of the phenyl ring and the carboxylate group. The Mn-MOF collected by heating the sample of 500°C. Maybe due to this, no such weight loss was observed until 600°C the solvent molecules were evaporated. There was no functional group peak at the figure, which shows the collapse of the compound due to the evaporation of solvent molecules at 1000°C. TGA curve of compound confirms the following points: (i) The Tpa molecules can be separated in the temperature range of 350–450°C and (ii) The framework formulated as Mn-MOF is constant in the temperature range 350–450°C.

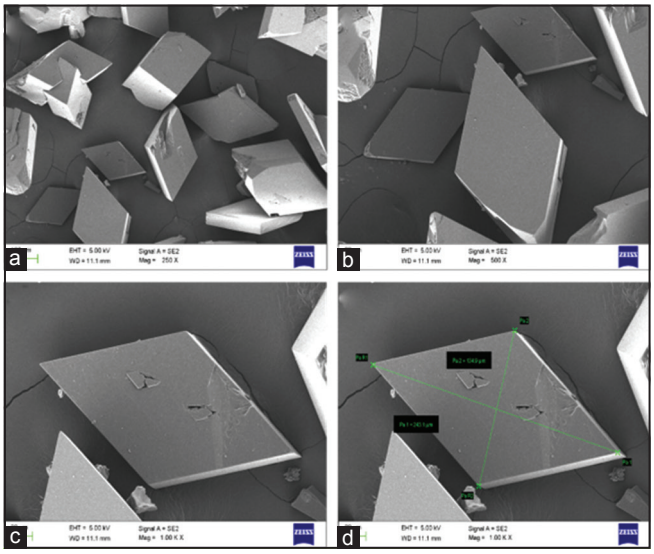

Figure 7: Field emission scanning electron microscope micrographs of manganese metal-organic framework crystals at different magnifications.

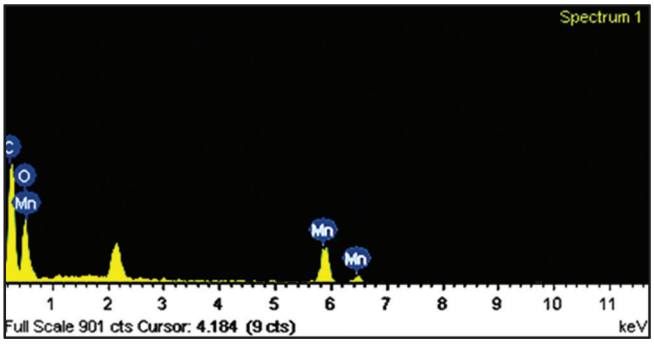

Figure 8: Energy dispersive X-ray pattern of manganese metal-organic framework.

4. ELECTROCHEMICAL STUDIES OF Mn-MOF

4.1. Preparation of Working Electrode (Mn-MOF/BCPE)

A paste of Mn-MOF sample (80 wt% or ~4 mg) was prepared with graphite powder (15 wt %) and polytetrafluoroethylene binder (5 wt%) along with a drop or two of ethanol. This mixture was consequently hand pressed on nickel mesh from all sides. Copper wire was used as the current collector. This electrode was left for drying at room temperature for about 24 h. The galvanostatic charge-discharge (GCD),

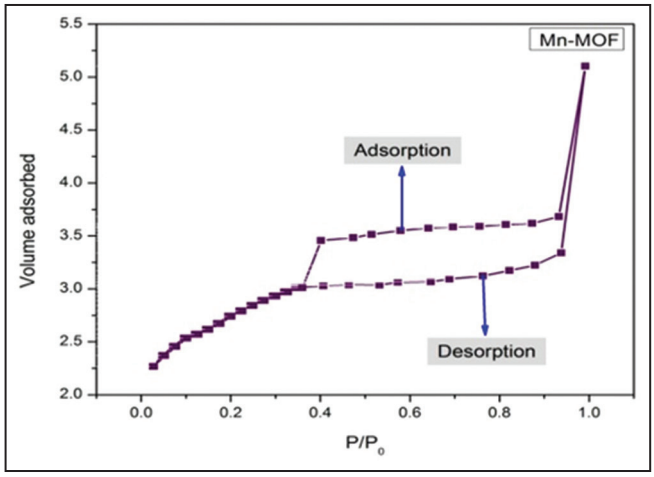

Figure 9: N_2 adsorption-desorption isotherms of manganese metal-organic framework compound.

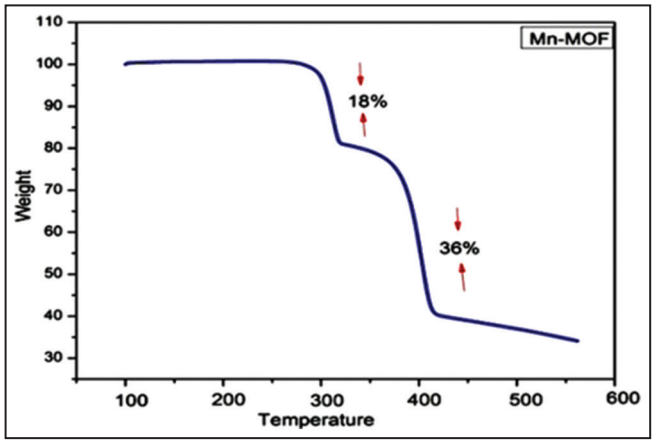

Figure 10: Thermogravimetry curve for the manganese metal-organic framework compound, which shows the weight loss regions of temperature.

cyclic voltammetry (CV), and impedance studies were made using 3 mol L^{-1} KOH electrolyte in a buffer solution on electrochemical (CHI 608E) instrument. The saturated calomel electrode, platinum (foil) electrode, and prepared Mn-MOF electrode were used as the reference, counter, and working electrodes, respectively [22].

4.2.1. CV study of Mn-MOF

Figure11a shows the cyclic voltammograms observed for the redox system of BCPE and Mn-MOF electrodes at the scan rate of 50 mVs^{-1}. A freshly prepared 10 mM of potassium ferricyanide with 0.5 M potassium chloride was placed in an electrochemical cell. The following reactions are given below.

$$Fe(CN)_6^{-4} \rightarrow Fe(CN)_6^{-3} + e \quad (1)$$

$$Fe(CN)_6^{-3} + e \rightarrow Fe(CN)_6^{-4} \quad (2)$$

The BCPE electrodes of anodic and cathodic peak potentials were 0.26 V and 0.17 V, respectively, and the difference of redox peak potential (ΔEp) was 0.09 V. The anodic and cathodic peak potentials of Mn-MOF are 0.334 V and 0.098 V and the ΔEp is 0.23 V. The Mn-MOF electrode shows a significant enhancement of redox peak current compared to BCPE. This indicates a very good electrocatalytic activity of Mn-MOF [23].

Figure 11b represents the cyclic voltammograms of Mn-MOF electrode at different scan rates (10–100 mVs^{-1}) with 5 mM of Fe^{2+}/Fe^{3+} system in 0.5 M KCl solutions.

The oxidation and reduction peak currents are directly proportional to the scan rate, which means that the reaction is surface restrained. These results indicate that the potentials for the oxidation peak and reduction peak shift to the positive and the negative direction, respectively, which could be mainly due to the internal resistance of the electrode [24].

Figure 12a shows the electrochemical behavior of the Mn-MOF, which was studied by CV in the potential range of −0.5–−0.1 V at different scan rates (10–200 mVs^{1}). The specific capacitance values were calculated using the following equation.

$$Cs = \frac{It}{\Delta Vm} \quad (3)$$

Where I is the average current for the both anodic and cathodic scan (A), m is the weight of the electroactive material from the electrode (g), and v is the scan rate (V).

The appearances of a couple of redox peaks in the CV curves indicate the pseudocapacitive behavior. The fine and sharp redox peaks of Mn-MOF can be exactly credited to the faradic reactions of the various oxidation states of Mn, and the route can be explained by the following reactions [25].

$$Mn(II)_S + OH^- \rightarrow Mn(II)_S\,(OH^-)ad + e^- \quad (4)$$

$$Mn(II)_S\,(OH^-)ad \rightarrow Mn(III)_S\,(OH^-)ad + e^- \quad (5)$$

The Mn-MOF material has shown the highest specific capacitance, which is due to the 3D network structure with large porosity and finest pore volume. These pores may be internal dynamic sites, which could improve the energy storage capacity of the electrode material. The specific capacitance of Mn-MOF electrode is calculated for different scan rates such as 10, 50, 100, 150, and 200 mvs^{-1}. The material exhibited the highest specific capacitance (Cs) of 270 Fg^{-1}at 10 mvs^{-1} in 3M KOH solution when compared to the available reports.

Figure 12b shows that the relationships between the graph of anodic peak current (Ipa) and square root of scan rate (v1/2) were plotted in the Mn-MOF electrode $R^2 = 0.988$. The specific capacitance is greatly reliant on the ion distribution of the electrolyte and charge transfer of the electrode surface by the adsorption of ions to the electrode materials. At a higher scan rate, this process may be quite slow and due to which there could be a decreased in the specific capacitance [26].

4.2.2. GCD study of Mn-MOF

Figure 12c exhibits the charge-discharge curves of Mn-MOF electrode. The GCD study was carried out within the potential range of 0.0–0.6 V

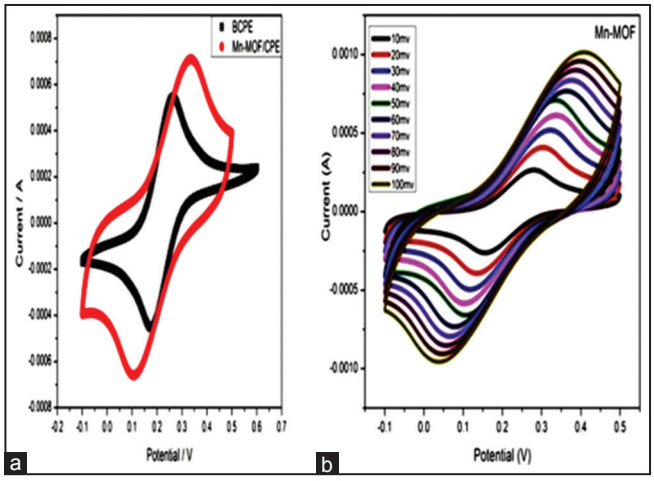

Figure 11: (a) Cyclic voltammetrys (CV) of bare carbon paste electrode/Manganese metal-organic framework (Mn-MOF) electrode at 50 mVs^{-1} scan rate and (b) CVs of Mn-MOF electrode in a mixture of 5 mM K_4FeCN_6 and $K_3FeCN_{6\,in}$ 0.5 M KCl solution at different scan rates such as 10–100 mVs^{-1}.

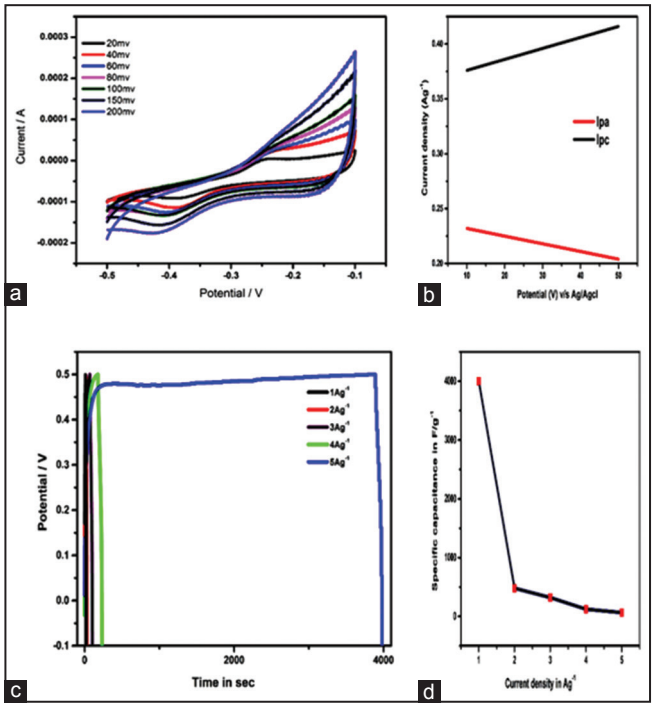

Figure 12: (a) Cyclic voltammetry of manganese metal-organic framework (Mn-MOF) electrode in a 3M KOH solution at different scan rates such as 10–100 mVs^{-1}, (b) relationships between the graph of anodic peak current (Ipa) and square root of scan rate (v1/2) were plotted in the Mn-MOF electrode, (c) galvanostatic charge/discharge curves with different current density, (d) specific capacity of Mn-MOF at various current densities.

at various current densities (1 Ag^{-1}, 2 Ag^{-1}, 3 Ag^{-1}, 4 Ag^{-1}, and 5 Ag^{-1}) to evaluate the cyclic stability and specific capacitance of Mn-MOF electrode. Figure 12d shows the increase in current with decreases in the specific capacitance. The specific capacitance was calculated using the following equation [27].

$$Csp = \frac{It}{m\Delta V} \quad (6)$$

Where C_{sp} (F/g) is the specific capacitance, I is the constant current (A) in the charge-discharge process, t is the discharge time (sec), m is the mass of the electroactive material (g), and ΔV (V) is the potential of Mn-MOF. The energy storage capacity Mn-MOF was estimated using the charge passed during the discharge process until a cut off potential was reached. This voltage was about 1 Ag^{-1} to 5 Ag^{-1}. We found that the specific capacitance varied from 4000 (F/g^{-1}), through 480 (F/g^{-1}), 321 (F/g^{-1}), 124 (F/g^{-1}), and 65 (F/g^{-1}) with an increase in current density. The energy density and power density of Mn-MOF electrode are 500.00 (Wh/kg^{-1}) and 0.125 (W/kg^{-1}), respectively (Figure 13a). These results imply the energy storage capacity of Mn-MOF electrode, which possesses a high charge-discharge columbic efficiency and also low polarization and high specific capacitance, including good cycling stability. The power density (P) and energy density (E) were calculated from the following equations:

$$\text{Power density, } P = \frac{E}{t} \quad (7)$$

$$\text{Energy density, } E = \frac{1}{2}CV^2 \quad (8)$$

Where C (F/g^{-1}), V (V), E (Wh/kg), P (W/kg), and t (s) are the specific capacitance, potential window, energy density, power density, and discharge time, respectively [26].

4.2.3. Electrochemical impedance studies of Mn-MOF

Electrochemical impedance spectroscopy study is another great tool for studying electron transfer between an electrode surface and electrolyte. Figure 13b shows the impedance graphs and matching equivalent circuits of a Mn-MOF electrode. In these graphs, the arc (semicircle) shows at elevated frequency region.

Here, Rct is the charge-transfer resistance, Cdl is the double layer capacitance, and W corresponds to the Warburg diffusion. This W is ascribed to the diffusion of ions. The equivalent circuits contain the solution resistance Rs, which is parallel to low-frequency capacitance, Rct. This spectrum consists of the semicircle with a lesser diameter at the high-frequency range. This is due to the charge transfer reaction [27,28]. The inclined linear part in the low-frequency range implies the Warburg impedance. With our electrode, no arc has appeared in the high-frequency region, which indicates the low charge resistance and high capacitance of our Mn-MOF electrode. The semicircles for the Mn-MOF at the high-frequency range are very small when compared to that of the BCPE. A smaller semicircle shows lesser charge-transfer resistance (Rct). Using the experimental data, the calculated values of Rct, Rs, Cdl, and W are 46.64 Ω, 15.58 Ω, 1.745×10^{-8} F, and 0.002127 Ω, respectively.

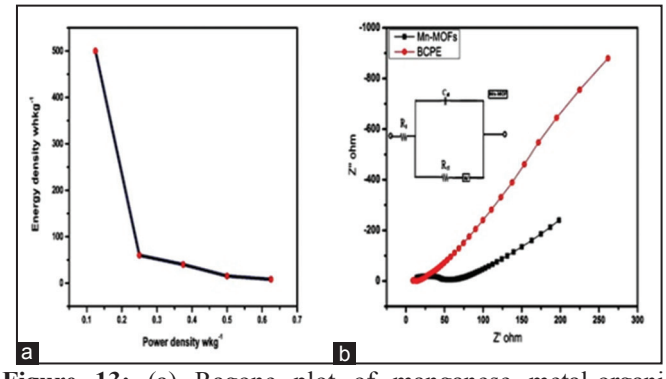

Figure 13: (a) Ragone plot of manganese metal-organic framework (Mn-MOF) composite, (b) Nyquist plot of bare carbon paste electrode and Mn-MOF electrodes equivalent circuits in 3M KOH solution.

5. CONCLUSION

The Mn-MOF, (Mn[Tpa][Mi][DMF]), has been successfully synthesized using terephthalic acid and methylimidazole ligands by the solvothermal method at a considerably low temperature of about 120°C. The accelerated formation of the product has been achieved in solvothermal condition. This could be due to the fast nucleation reaction, whereas, in a conventional heating method, the nucleation takes place only on the walls of the reaction container. Furthermore, the solvothermal method provides a uniform nucleation environment for the crystal growth. A very interesting morphology of the product this been found from the SEM images. The crystal/particle dimensions are in the range of 100 µm and 20 µm. The particles are having the surface area of 2352 m^2/g and the pore volume of 0.00569 cc/g. The surface area of this material is quite prominent when compared to the reported similar kind of MOFs, which can be of great significance for Energy (H_2 gas) storage application. The observed charge storage (specific) capacitance was up to 4000 (F/g). It varies inversely with the current density between 4000(F/g) and 65(F/g). Using the experimental data, the calculated energy density and power density of this Mn-MOF material are 500.00 (wh/kg) and 0.125 (w/kg), respectively. These results indicate that our Mn-MOF electrode yields high charge-discharge columbic efficiency, low polarization, and high specific capacitance along with good cycling stability. Thus, our MOF is a better energy storage material.

6. ACKNOWLEDGMENTS

The authors like to acknowledge Bangalore University (Scheduled Caste and Scheduled Tribes cell) for financial support (fellowship). Authors acknowledge the University Grants Commission/Department of Science and Technology, India, for the Instrumental facilities at our department premises to carry out this research work. We also like to acknowledge Dr. P. Raghavendra Kumar, University College of Science at Tumkur University for the CV study.

Supplementary Material

The CCDC number of the material is 1,564,429, which provides the supplementary crystallographic data have been deposited with the CCDC, CCDC No. 1564429. The information may be obtained by, The Director, CCDC, Cambridge CB2 1EZ, 12 Union Road, UK (fax: +44–1223–336–033; e-mail: deposit@ccdc.cam.ac.uk).

7. REFERENCES

1. J. Pang, E. J. P. Marcotte, C. Seward, R. S. Brown, S. Wang, (2001) A blue luminescent star-shaped Zn II complex that can detect benzene, ***Angewandte Chemie International Edition***, **40:** 4042.
2. J. Y. Lu, J. Li, M. A. Lawandy, (1999) A new type of two-dimensional metal coordination systems: Hydrothermal synthesis and properties of the first oxalate bpy mixed-ligand framework [M(ox)(bpy)] (M = Fe(II), Co(II), Ni(II), Zn(II); ox = C_2O_4-; bpy = 4,4‘-bipyridine), ***Journal of Inorganic Chemistry***, **38:** 2695.

3. I. J. Dance, (2007) The mechanistically significant coordination chemistry of dinitrogen at femo-co, the catalytic site of nitrogenase, ***American Chemical Society***, **129:** 1076-1088.
4. T. K. Maji, G. Mostafa, H. C. Chang, S. Kitagawa, (2005) Porous lanthanide organic framework with zeolite-like topology, ***Chemical Communications***, **19(9)**: 2436-2438.
5. J. Jin, W. Y. Wang, Y. H. Liu, H. W. Hou, Y. T. Fan, (2011) STM studies of single molecules: Molecular orbital aspects, ***Chemical Communications***, **47:** 2762.
6. K.S. Murray, (1995) Advanced in Inorganic Chemistry, Vol. 43. San Diego, USA: Academic Press, p261.
7. G. Krishnamurthy, B. M. Omkaramurthy, (2016) Zinc metal-organic frameworks: The advanced/energy materials prepared from terephthalic acid and methyl imidazole by solvothermal method, ***Journal of Electrochemical Society of India,*** **13-466**: 164-169.
8. M. Casarin, A. Cingolani, C. D. Nicola, D. Falcomer, M. Monari, L. Pandolfo, C. Pettinari, (2007) Systematic synthesis of a metal organic framework based on triangular $Cu_3(\mu_3\text{-}OH)$ secondary building units: From a 0-D complex, to an 1-D chain and a 3-D lattice, ***Crystal Growth and Design***, **4:** 676.
9. G. Ferey, (2008) Hybrid porous solids: Past, present, future, ***Chemical Society Review***, **37:** 191-214.
10. N. Stock, S. Biswas, (2011) Synthesis of metal-organic frameworks (MOFs): Routes to various MOF topologies, morphologies, and composites, ***Chemical Review***, **112:** 933-969.
11. M. Wang, Y. R. Zheng, K. Ghosh, P. J. Stang, (2010) Post-self-assembly covalent chemistry of discrete multicomponent metallo supramolecular hexagonal prisms, ***Journal of American Chemical Society***, **132:** 6282.
12. A. X. Tian, J. Ying, J. Peng, J. Q. Sha, H. J. Pang, P. P. Zhang, Y. Chen, M. Z. Zhu, M. Su, (2009) Two new Keggin-type polyoxometalate-based organic-inorganic hybrid compounds with metal ions and chelate ligands, ***Inorganic Chemistry***, **48:** 100.
13. T. J. Burchell, R. J. Puddephatt, (2005) Self-assembly of chiral coordination polymers and macrocycles: A metal template effect on the polymer macrocycle equilibrium, ***Inorganic Chemistry***, **44:** 3718.
14. H. F. Zeng, T. H. Li, Z. W. Yan, S. J. Luo, F. Li, (2010) Chelating ligand-mediated crystal growth of cerium orthovanadate, ***Crystal Growth Design***, **10:** 475.
15. Q. K. Liu, J. P. Ma, Y. B. Dong, (2010) Color tuneable and white light emitting Tb^{3+} and Eu^{3+} doped lanthanide metal organic framework materials, ***Journal of American Chemical Society***, **132:** 7005.
16. J. L. C. Rowsll, O. M. Yaghi, (2005) Strategies for hydrogen storage in metal organic frameworks, ***Angewandte Chemie International Edition***, **44:** 4670-4679.
17. L. J. Murray, M. Dinca, J. R. Long, (2009) Metal-organic frameworks as sensors: A ZIF-8 based fabry-pe´ rot device as a selective sensor for chemical vapors and gases, ***Chemical Society Reviews***, **38:** 1294-1314.
18. D. J. Collins, H. C. Zhou, (2007) Hydrogen storage in metal organic frameworks, ***Journal of Material Chemistry***, **17:** 3154-3160.
19. K. M. Thomas, (2009) Adsorption and desorption of hydrogen on metal organic framework materials for storage applications: Comparison with other nanoporous materials, ***Dalton Transactions***, **120:** 1487-1505.
20. V. I. Isaeva, L. M. Kustov, (2007) Metal-organic frameworks-new materials for hydrogen storage, ***Russian Journal of General Chemistry***, **77:** 721-739.
21. X. J. Lin, P. H. Jia, P. Hubberstey, M. Schroder, N. R. Champness, (2007) Hydrogen storage in metal organic frameworks, ***Crystal Engineering Communications***, **9:** 438-448.
22. K. M. Thomas, (2007) Hydrogen adsorption and storage on porous materials, ***Catalysis Today***, **120:** 389-398.
23. L. Wang, Z. H. Dong, Z. G. Wang, F. X. Zhang, J. Jin, (2013) Layered $\alpha\text{-}Co(OH)_2$ nanocones as electrode materials for pseudocapacitors: Understanding the effect of interlayer space on electrochemical activity, ***Advanced Functional Materials***, **13:** 2758-2764.
24. D. Zhao, H. C. Y. Zhou, (2008) The current status of hydrogen storage in metal organic frameworks, ***Energy Environmental Science***, **1:** 222-235.
25. G. Krishnamurthy, M. S. Shivakumar, (2017) Electroless deposition of nanosized nickel over graphite substrate with better coating coverage and catalytic activity for fuel cell application, ***Journal of Applied Electrochemistry***, **47:** 519-529.
26. R. Shah, X. F. Zhang, S. Talapatra, (2009) Materials made of carbon nanotubes. The carbon nanotube forest, ***Nanotechnology***, **395:** 202-395.
27. G. Krishnamurthy, B. M. Omkaramurthy, S. Sangeetha, (2017) Mn and Co, metal - organic frameworks for hydrogen gas (energy) storage and heavy metal ion sensor application for clean environment, ***International Journal of Science and Engineering Management*****, 2:** 159-162.
28. Y. Zhang, G. L. Y. Li, L. Wang, A. Zhang, Y. Song, B. Huang, (2011) Electrochemical investigation of MnO_2 electrode material for supercapacitors, ***International Journal of Hydrogen Energy***, **36:** 11760-11766.

****Bibliographical Sketch***

Dr. G. Krishnamurthy, M.Sc., M.Phil., Ph.D. Assistant Professor, Department of Studies in Chemistry, Bangalore University, Central College Campus, Bangalore-560061, Mob. Ph: +919449523166 E-mail: drgkmurthy.bub@gmail.com . Research area- H2 Storage Nano materials: Carbon nanotubes, Carbon spheres, Metal Organic frameworks and their energy storage properties